8-1-2022

Collagen VII Maintains Proteostasis in Dermal Fibroblasts by Scaffolding TANGO1 Cargo

Qingqing Cao

Grace Tartaglia

Michael Alexander

Pyung Hung Park

Shiv Poojan

See next page for additional authors

Authors

Qingqing Cao, Grace Tartaglia, Michael Alexander, Pyung Hung Park, Shiv Poojan, Mehdi Farshchian, Ignacia Fuentes, Mei Chen, John . A. McGrath, Francis Palisson, Julio Salas-Alanis, and Andrew P. South

Collagen VII maintains proteostasis in dermal fibroblasts by scaffolding TANGO1 cargo

Qingqing Cao [a], Grace Tartaglia [a], Michael Alexander [a], Pyung Hung Park [a], Shiv Poojan [a], Mehdi Farshchian [a], Ignacia Fuentes [b,c], Mei Chen [d], John A. McGrath [e], Francis Palisson [b,f], Julio Salas-Alanis [g] and Andrew P. South [a,h,i]

***a* - Department of Dermatology and Cutaneous Biology,** *Thomas Jefferson University, Philadelphia, PA*
***b* - DEBRA Chile,** *Santiago, Chile*
***c* - Centro de Genética y Genómica,** *Facultad de Medicina Clínica Alemana, Universidad de Desarrollo, Santiago, Chile*
***d* - Department of Dermatology,** *The Keck School of Medicine at the University of Southern California, Los Angeles, CA*
***e* - St. John's Institute of Dermatology,** *King's College London (Guy's Campus), UK*
***f* - Facultad de Medicina Clínica Alemana,** *Universidad de Desarrollo, Santiago, Chile*
***g* - Instituto Dermtaologico de Jalisco,** *Guadalajara, Mexico*
***h* - The Joan and Joel Rosenbloom Research Center for Fibrotic Diseases,** *Thomas Jefferson University, Philadelphia, PA*
***i* - Sidney Kimmel Cancer Center,** *Thomas Jefferson University, Philadelphia, PA*

Corresponding author at: *Thomas Jefferson University, 233 S. 10th Street, BLSB 406, Philadelphia, PA 19107.*
Andrew.south@Jefferson.edu.
https://doi.org/10.1016/j.matbio.2022.06.008

Abstract

Lack of type VII collagen (C7) disrupts cellular proteostasis yet the mechanism remains undescribed. By studying the relationship between C7 and the extracellular matrix (ECM)-associated proteins thrombospondin-1 (TSP1), type XII collagen (C12) and tissue transglutaminase (TGM2) in primary human dermal fibroblasts from multiple donors with or without the genetic disease recessive dystrophic epidermolysis bullosa (RDEB) (n=31), we demonstrate that secretion of each of these proteins is increased in the presence of C7. In dermal fibroblasts isolated from patients with RDEB, where C7 is absent or defective, association with the COPII outer coat protein SEC31 and ultimately secretion of each of these ECM-associated proteins is reduced and intracellular levels are increased. In RDEB fibroblasts, overall collagen secretion (as determined by the levels of hydroxyproline in the media) is unchanged while traffic from the ER to Golgi of TSP1, C12 and TGM2 occurs in a type I collagen (C1) dependent manner. In normal fibroblasts association of TSP1, C12 and TGM2 with the ER exit site transmembrane protein Transport ANd Golgi Organization-1 (TANGO1) as determined by proximity ligation assays, requires C7. In the absence of wild-type C7, or when ECM-associated proteins are overexpressed, C1 proximity and intracellular levels increase resulting in elevated cellular stress responses and elevated TGFβ signaling. Collectively, these data demonstrate a role for C7 in loading COPII vesicle cargo and provides a mechanism for disrupted proteostasis, elevated cellular stress and increased TGFβ signaling in patients with RDEB. Furthermore, our data point to a threshold of cargo loading that can be exceeded with increased protein levels leading to pathological outcomes in otherwise normal cells.

Introduction

The rare and devastating genetic skin disease recessive dystrophic epidermolysis bullosa (RDEB) is caused by mutations in the gene encoding type VII collagen (C7) [1]. RDEB is characterized by skin and mucosal fragility, chronic wounds, extensive tissue fibrosis, and the eventual development of life-

threatening skin cancers [2,3]. C7 is the largest collagen molecule and the major component of anchoring fibrils, supramolecular structures that aid adhesion between the epidermal layer of the skin and underlying dermis [4]. In addition to supporting epidermal-dermal adhesion, C7 also plays important signaling roles in the skin and other tissues and recent work has described increased TGFβ signaling and altered proteostasis as a result of absent or dysfunctional C7 found in patients with RDEB [5–12]. While published studies have provided potential mechanisms for increased TGFβ signaling in RDEB, no mechanism for the observations of disrupted vesicle traffic and global changes to ECM composition have been proposed.

Like all collagens, the procollagen form of C7 is synthesized and processed in the endoplasmic reticulum (ER), and in turn is transported in a coat protein II complex (COPII)-dependent manner to the Golgi [13]. Now decade old work identified a specialized COPII secretory mechanism capable of transporting cargo presumed larger than standard COPII vesicle diameters of 60-90nm [14,15]. These so-called COPII large carriers were reported to be facilitated by Transport ANd Golgi Organization-1 (TANGO1), a transmembrane protein located at ER exit sites and described as essential for C7 export from dermal fibroblasts [14]. Subsequent work has shown that TANGO1 promotes cargo loading by interacting with both the cargo and the inner coat of COPII vesicles (SEC23 and SEC24), delaying the recruitment of the outer coat proteins (SEC13 and SEC31) until cargo is loaded [16,17]. Given that pro-collagen C7 is around 400nm in length and much larger than other collagens such as type I collagen (C1) which has been shown to be secreted independent of TANGO1 in dermal fibroblasts [14], the existence of large carriers provides a plausible explanation for transport of bulky cargo. However, existence of large carriers has not been observed in all experimental systems used to address ER to Golgi transport and much remains unknown with regards to molecular mechanisms required to sort, correctly modify and distribute proteins through the ER-Golgi system and in different cell types [18,19]. Indeed, while work in dermal fibroblasts demonstrate a specific role for TANGO1 in C7 secretion, independent of C1, studies in other cellular systems suggest a wider role for TANGO1 in secretion [20,21].

Disruption to cellular proteostasis in dermal fibroblasts has been reported in RDEB through the use of mRNA and elegant proteomic studies [6,7,10,11]. Loss of collagen VII has been associated with perturbed vesicular traffic, with increases in COPI and COPII components, as well as reduced autophagic flux, indicating alterations to cellular stress responses in RDEB fibroblasts [10]. Two proteins with substantial influence on the tissue microenvironment that have been shown to directly bind C7 in normal fibroblasts and are disrupted in RDEB are thrombospondin-1 (TSP1) and tissue transglutaminase (TGM2) [5,10]. TGM2 levels are shown to be reduced in RDEB patients and associated with diminished adhesion, perturbed autophagy and reduced cross-linking of the ECM [10]. However, the association between reduced TGM2 and perturbed autophagic flux is based on separate observations in murine and other cellular systems [22,23] without demonstration of a direct role for TGM2 in RDEB beyond binding C7 [10]. In contrast, TSP1, a large homotrimeric glycoprotein with a complex and extensive interactome [24], facilitates an array of diverse roles in multiple tissue microenvironments and pathologies [25], and is significantly upregulated in RDEB correlating with disease severity [5–8]. One prominent role for TSP1 is activation of transforming growth factor-beta (TGFβ) signaling revealed by the overlapping phenotypes of thbs1 -/- and tgfb1 -/- mice studies [26] and by studies identifying binding between TSP1 and the TGFβ latent-associated protein (LAP) complex facilitating release of extracellular matrix-bound TGFβ ligand [27,28]. We have previously demonstrated that absence of C7 leads to increased bioavailability of TSP1 in the dermal microenvironment concomitant with increased TGFβ signaling [5].

Here we use primary dermal fibroblasts isolated from multiple donors with (n=15) or without (n=16) RDEB to determine the mechanism behind the relationship between C7 and ECM-associated protein secretion. We describe the close proximity of TSP1, TGM2 and type XII collagen (C12) with two separate collagen molecules, C1 and C7, in the context of COPII secretion and eventual exit from the cell. We demonstrate that proximity of ECM-associated proteins with TANGO1 requires C7. In the absence of wild type C7, ECM-associated protein secretion is reduced along with a concordant increased proximity with C1, increased ER stress, and elevated TGFβ signaling. We also show that C7-associated secretion in normal cells has a threshold of capacity which, when exceeded, leads to concurrent cellular stress and TGFβ signaling.

Results

Wild-type C7 directs ECM protein secretion in dermal fibroblasts

Our previous work using recombinant HSV-1 virus, which transiently delivers high levels of C7 to dermal fibroblasts, implicated a potential role for C7 in TSP1 secretion [5]. The direct effect of C7 on TSP1 secretion had been previously unobserved using retroviral delivery of C7 where low transduction efficiencies require antibiotic selection over a 2-3 week period by which time TGFβ signaling and TSP1 expression, a TGFβ target, had diminished

[7]. In agreement with a role for C7 in TSP1 secretion, primary fibroblasts isolated directly from RDEB patients showed a greater ratio of intracellular to extracellular TSP1 compared with primary normal dermal fibroblasts (*Figure 1A*). This difference between RDEB and normal fibroblasts was reversed after expression of full length C7 in RDEB fibroblasts, identifying TSP1 secretion is altered by the absence of functional C7 (*Figure 1A*). This observation extended to two other ECM-associated proteins shown to be altered in RDEB, tissue transglutaminase (TGM2) and type XII collagen (C12) (*Figure 1B*).

To evaluate the relationship between TSP1, TGM2, C12 (referred to herein as ECM-associated proteins) and the COPII secretory pathway, we examined the close proximity between each individual protein and SEC31, the COPII outer coat protein indicative of COPII vesicle maturation, using proximity ligation assay (PLA), a method to detect protein-protein associations within 40nm in situ [29] (*Figure S1A*). In RDEB fibroblasts, SEC31 expression, SEC31 – SEC23 co-localization, and overall collagen secretion (as determined by hydroxyproline levels) was not affected by the absence of C7 (*Figure S1B & C*), but co-localization between ECM-associated proteins and SEC31, measured by PLA, was: proximity between TSP1 and SEC31, TGM2 and SEC31, and C12 and SEC31, were all significantly reduced in RDEB fibroblasts compared with normal and re-expression of C7 restored SEC31 proximity (*Figure 1C*), indicating that co-localization of TSP1, TGM2 and C12 with SEC31 is regulated by C7. TSP1 was in close proximity with both TGM2 and C12 in normal fibroblasts and this proximity was reduced in RDEB fibroblasts (*Figure S1D*). Taken together, these observations suggest that COPII secretion of ECM-associated proteins in dermal fibroblasts is modulated by C7. Furthermore, secretion of TSP1 and co-localization between TSP1 and SEC31 reduced with increasing disease severity in primary RDEB fibroblasts (*Figure 1D*, *1E* and *Table 1*), implying that impaired SEC31 proximity and protein secretion correlates with RDEB patient phenotype. Taken together, these observations suggest that COPII secretion of ECM-associated proteins in dermal fibroblasts is in part C7 dependent, and correlates with RDEB disease severity.

TANGO1 association with TSP1, TGM2 and C12 is dependent on the presence of C7

We next investigated the relationship between C7, ECM-associated proteins and TANGO1, since TANGO1 is reported to mediate both C7 and C12 secretion in dermal fibroblasts [14,30]. Similar to C7, TSP1 co-localized with TANGO1 in normal dermal fibroblasts but was significantly reduced or did not co-localize in RDEB fibroblasts (*Figure 2A* and *Figure S2A*). To investigate whether TANGO1 is important for SEC31 proximity and secretion, we silenced TANGO1 using siRNA in both normal and RDEB fibroblasts and analyzed TSP1, TGM2 and C12 proximity with SEC31. Proximity between TSP1 and SEC31 was significantly diminished after silencing TANGO1 in normal fibroblasts, but this reduction was not observed in RDEB fibroblasts (*Figure 2B*). siRNA knock down of TANGO1 resulted in decreased secretion of TSP1, TGM2 and C12 in normal dermal fibroblasts without significant change in RDEB (*Figure 2C*). siRNA knock down of C7 also reduced TGM2 and C12 secretion in normal cells (*Figure 2D*). To control for any off-target effects of lipid transfection we compared TSP1 secretion with or without siRNA mock transfections and saw no changes to TSP1 (*Figure S2B*). Finally, TGM2-TANGO1 PLA and C12-TANGO1 PLA is reduced in RDEB and restored after C7 expression (*Figure 2E*). Overall, these results identify that TSP1, TGM2 and C12 proximity with TANGO1 is dependent on C7 in dermal fibroblasts and that in the absence of TANGO1 or functional C7, secretion is reduced.

ECM proteins associate with collagen I in the absence of C7 or when ectopically expressed

Since TSP1 is secreted in RDEB fibroblasts and is shown to activate TGFβ through extracellular binding of TGFβ-LAP in RDEB patients [5], we hypothesized that secretion of TSP1 in the absence of C7 likely traffics through a separate mechanism. Because type I collagen (C1) is reported to be secreted in a TANGO1-independent manner in dermal fibroblasts [14], we investigated a possible relationship between ECM-associated proteins and C1 in RDEB. We first confirmed that siRNA knockdown of TANGO1 did not affect C1 secretion in RDEB (*Figure S2C*) and that C1 secretion was not significantly altered, as measured by the ratio of intracellular to extracellular protein (*Figure S2D*), in agreement with no change to global collagen levels in RDEB (*Figure S1C*). No detectable PLA signals were observed between C1 and C7 (*Figure S2E*) and confocal microscopy confirmed that these proteins show a lower co-localization correlation when compared with SEC31 (*Figure S2F*). The lack of C1 and C7 proximity is not a result of differential antibody binding since C1-SEC31 PLA and C7-SEC31 PLA are readily detected in normal dermal fibroblasts (*Figure S2E*). We used PLA to assess the proximity of ECM-associated proteins and C1, beginning with TSP1, and observed that in normal dermal fibroblasts, C1 showed very

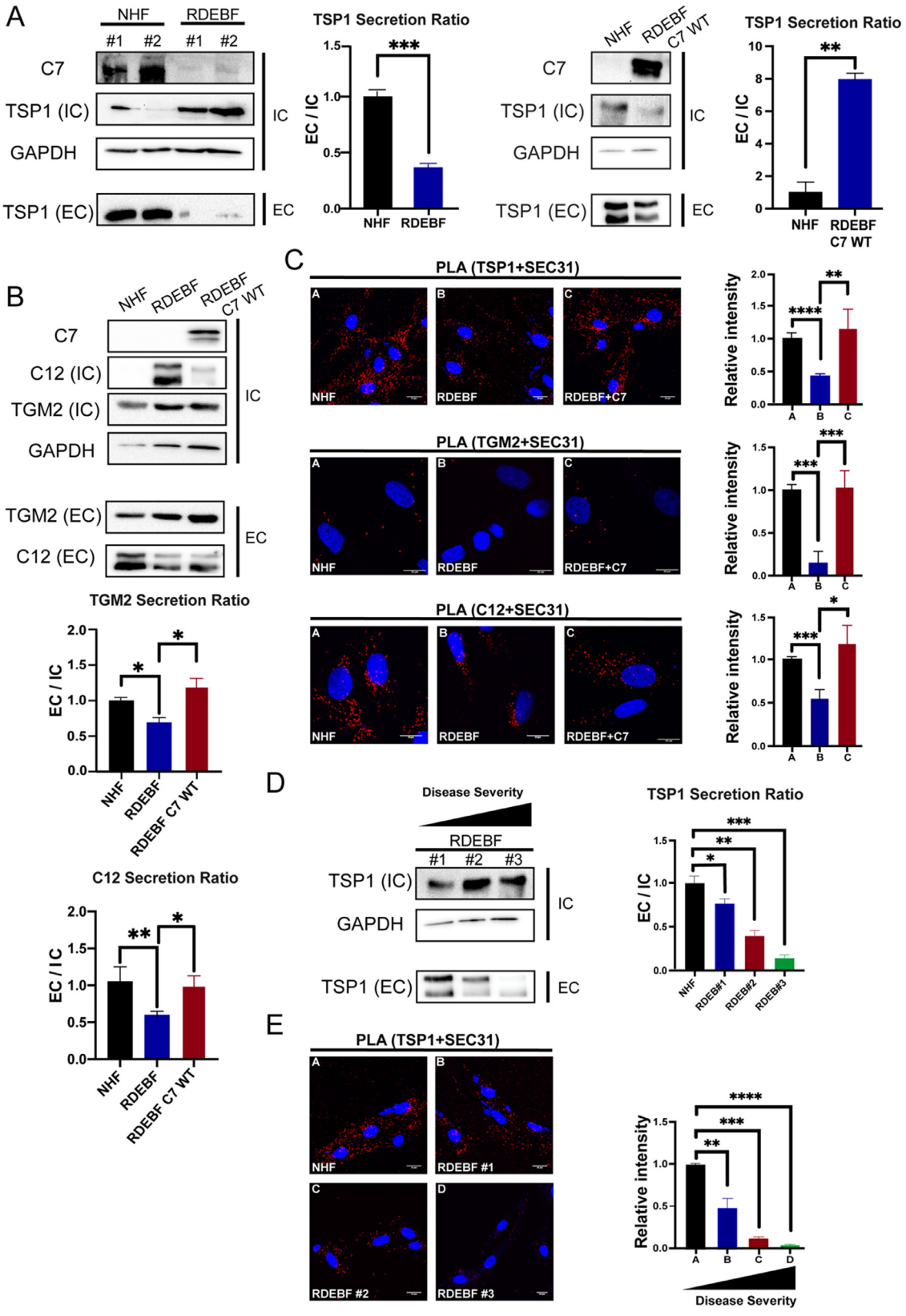

Figure 1. Wild-type C7 directs ECM-associated protein secretion. (**A**). Left: Immunoblot of type VII collagen (C7), and TSP1 from total cell lysates (intracellular; IC) and conditioned media (extracellular; EC) from primary normal human

little proximity with TSP1 compared to RDEB fibroblasts where C1 and TSP1 demonstrated strong PLA signals (*Figure 3A*). PLA between C1 and TSP1 was significantly reduced in RDEB fibroblasts after expression of recombinant C7 (*Figure 3A*), confirming that TSP1 – C1 proximity increases in the absence of C7. Next, we used siRNA knockdown of C1 and observed a significant reduction in TSP1 secretion in RDEB fibroblasts demonstrating that in the absence of functional C7, TSP1 secretion is in part dependent on C1 (*Figure 3B*). Using a similar approach and comparing C1 knock-down with C7 knockdown in normal fibroblasts we show a reduction in TSP1 secretion after C1 knock-down and a further decrease in TSP1 secretion with C7 knockdown (*Figure 3C*), suggesting that C7-dependent secretion is the primary pathway to export TSP1 in normal fibroblasts but both secretory pathways can be utilized. In agreement with this idea, siRNA silencing of both TANGO1 and C1 in normal dermal fibroblasts led to the lowest level of TSP1 secretion compared to individual knockdown (*Figure 3D*). Collectively, these data suggest that TSP1 can traffic via two independent pathways. We next investigated if the same was true for TGM2 since levels of secreted TGM2 are reported to be significantly reduced in RDEB compared with normal [10]. We readily detected PLA between TGM2 and C1 in RDEB and this PLA signal was absent in normal and abolished in RDEB after re-expression of C7 (*Figure 3E*). Finally, and to determine whether ectopic overexpression of TSP1 could saturate C7-mediated TSP1 secretion in normal fibroblasts and lead to an association of TSP1 with C1, we expressed recombinant TSP1 in normal fibroblasts using a transient CMV driven system. Increased TSP1 in normal fibroblasts led to an increase in TSP1 – C1 proximity (*Figure 3F*) in the absence of changes to TSP1 – TANGO1 proximity (*Figure 3G*). Increased TSP1 in normal dermal fibroblasts also lead to reduction in C12 secretion in the absence of changes to C1 suggesting that saturation of the C7-mediated pathway reduces efficiency of this pathway (*Figure 3H*).

Taken together, these results indicate that ECM-associated proteins are primarily exported via a C7-dependent pathway while traffic associated with C1 proximity is accessible for export and increased when C7 is absent or when ECM-associated proteins are increased, presumably as a result of saturating the C7-dependent pathway.

C7 binding promotes ECM-associated protein – SEC31 proximity and increased secretion

We next examined whether binding to C7 promoted ECM-associated protein secretion and proximity to SEC31 in RDEB fibroblasts by expressing a mutant version of C7 lacking the reported TSP1 binding domain, the fibronectin III-like repeats 6 and 7 [31] (*Figure 4A*). We previously demonstrated binding between C7 and TSP1 using surface plasmon resonance, PLA and immuno-precipitation [5]. Here, using immuno-precipitation, we confirmed that the mutant C7 associated with TANGO1 but failed to show strong association with TSP1 (*Figure 4B*). Mutant C7 was efficiently secreted (*Figure 4B*) but failed to promote close proximity between TSP1 and SEC31 (*Figure 4C*), TSP1 secretion (*Figure 4D*), or a significant reduction in TGFβ signaling (as indicated by phosphorylated SMAD3) compared with wild type C7 in RDEB fibroblasts (*Figure 4D*). Mutant C7 was able to induce TANGO1 – TGM2 PLA and abrogate TGM2 – C1 PLA in RDEB fibroblasts to the same extent as wild-type C7 (*Figure S3A*), confirming that lack of C7-TSP1 association directly results in the TSP1 secretory defect observed in RDEB fibroblasts. In agreement with these data we confirmed that both mutant and wild type C7 precipitated a complex containing TGM2 (*Figure S3B*). These data demonstrate that C7 – TSP1

fibroblasts (NHF) and primary RDEB patient fibroblasts (RDEBF). Quantification graph showing ratios of extracellular to intracellular TSP1 densitometry relative to GAPDH from 2 separate primary fibroblast populations. Mean ± SEM from replicate experiments (n=3), ***: $p<0.001$. Right: Immunoblot of intracellular and extracellular TSP1 from NHF and RDEBF with recombinant wild-type C7 expression. Graph shows densitometry ratios of extracellular to intracellular TSP1 from immunoblot quantification. Mean ± SEM from replicate experiments (n=3), **: $p<0.01$. (**B**). Immunoblot of C7, type XII collagen (C12) and transglutaminase 2 (TGM2) from cell lysate (IC) and conditioned media (EC) from NHF, RDEBF and RDEBF expressing recombinant wild-type C7. Quantification graphs showing ratios of extracellular to intracellular TGM2 and C12 densitometry relative to GAPDH. Mean ± SEM from replicate experiments (n=3), *, $p<0.05$, **, $p<0.01$ (**C**). Proximity Ligation Assay (PLA) between TSP1/SEC31, TGM2/SEC31 and C12/SEC31. 30 cells were counted in each experiment. Scale bar: 20μm. Graphs show mean ± SEM from replicate experiments (n=3), *: $p<0.05$, **: $p < 0.01$, ***: $p<0.001$, ****, $p<0.0001$. (**D**) Immunoblot of intra- and extra-cellular TSP1 of RDEBF from three different patients with increasing disease severity (see ***Table 1*** for full details). Samples were run on the same blot as **1A** and quantified relative to NHF. Quantification graph showing ratios of extracellular to intracellular TSP1. Mean ± SEM from replicate experiments (n=3), *: $p<0.05$, **: $p < 0.01$, ***: $p<0.001$. (**E**). Left: PLA between TSP1 and SEC31 measured in primary NHF and three RDEB patient fibroblasts with different mutations and disease severity: top panels show NHF and generalized (intermediate) RDEB while bottom panels show severe generalized RDEB (see ***Table 1*** for full details). 20 cells were counted in each experiment. Scale bar: 20 μm. Data are shown as mean ± SEM from replicate experiments (n=3). **: $p < 0.01$, ***: $p<0.001$, ****, $p<0.0001$.

Table 1. Patient cells used in this study.

Patient	Cell Name	COL7A1 Mutation	Figure Reference
Breast reduction	BR23	Wild type	Figure S1C
Breast reduction	BR28	Wild type	Figure 2A, 5C, 5D
Breast reduction	BR31	Wild type	Figure S1C
Breast reduction	BR47	Wild type	Figure 3E, 3F, S1C
Breast reduction	BR49	Wild type	Figure 3G, S1B
Breast reduction	BR52	Wild type	Figure 2A, 2B, 3C, 3D
Breast reduction	BR59	Wild type	Figure 1C, S1C, S2B, S2E S4B
Breast reduction	BR71	Wild type	Figure S2F
Breast reduction	BR77	Wild type	Figure 3H, 5C
Breast reduction	BR79	Wild type	Figure S2C
Breast reduction	BR81	Wild type	Figure S1B, S2D
Breast reduction	BR84	Wild type	Figure 5B
Breast reduction	BR87	Wild type	Figure 1A, 3H, 5D, S1D
Breast reduction	BR90	Wild type	Figure 1E, S2A, S2B, S3B
Breast reduction	BR91	Wild type	Figure 1A, 1B, 2C, 2E
Breast reduction	BR92	Wild type	Figure 2D, 3A, S1C, S2A
Severe RDEB	RDEB13	p.G2073D/p.R578X	Figure 1D, 1E
Severe RDEB	RDEB70	c.425 A>G, p.K142R / c.425 A>G, p. K142R	Figure 1A, S1B
Severe RDEB	RDEB75	N/A	Figure 2A
Intermediate RDEB	RDEB79	c.2471dupG / c.2471dupG	Figure 1A
Intermediate RDEB	RDEB80	c.2471dupG / c.2471dupG	Figure S1C, S2A
Severe RDEB	RDEB83	c.C4373T:p.P1458L / c.5772+1delG	Figure S2B, S2C
Severe RDEB	RDEB84	c.8709del11/ G2899del11_fs. / c.8709del11/ G2899del11_fs.	Figure S1B
Intermediate RDEB	RDEB85	c.2044C>T:p.R682X / c.6101G>C:p. G2034A	Figure 1D, 1E, 2A, S1C, S3C
Intermediate RDEB	RDEB86	N/A	Figure 2B
Severe RDEB	RDEB103	N/A	Figure 5A, 5C, S1C, S1D, S4
Severe RDEB	RDEB104	N/A	Figure S2B, S4B
Severe RDEB	RDEB118	c.1732C>T:p.R578X / c.7474C>T: p. R2492X	Figure 2C, 3B, 3D, S1C, S2A
Intermediate RDEB	RDEB119	c.5565_5568+8delinsA / c.6527insC:p. G2177WfsX113	Figure 1D, 1E, 5A, S1C, S2C
Severe RDEB	RDEB121	c.1732C>T: p.R578X / c.7786delG: p. G2596VfsX33	Figure 1B, 1C, 2E, 3A, 3E, S3A,
Severe RDEB	RDEB123	c.6527insC: p.G2177WfsX113 / c.6527insC: p.G2177WfsX113	Figure 5B, S1A, S2A, S4
Severe RDEB	RDEB121 WT C7	c.1732C>T: p.R578X / c.7786delG: p. G2596VfsX33	Figure 1A, 1B, 1C, 2E, 3A, 3E, 4B, 4C, 4D, S2E, S2F,S3A, S3B
Severe RDEB	RDEB121 mutant C7	c.1732C>T: p.R578X / c.7786delG: p. G2596VfsX33	Figure 4B, 4C, 4D, S3A, S3B
Severe RDEB	RDEB121 antisense C7	c.1732C>T: p.R578X / c.7786delG: p. G2596VfsX33	Figure 4B, 4C, 4D

association facilitates loading of TSP1 into TANGO1 mediated COPII vesicles and absent C7 – TSP1 association leads to reduced TSP1 secretion, increased TSP1-C1 proximity, and increased TGFβ signaling. Given our previous work confirming TSP1-C7 immuno-precipitation with surface plasmon resonance we infer that this association is a result of direct binding between C7 and TSP1.

Intracellular levels of ECM-associated proteins correlate with increased TGFβ activation and increased cellular stress response in RDEB fibroblasts

Since intracellular levels of TSP1 correlate with increased p-SMAD3 levels in RDEB fibroblasts (*Figure 4D*) and ER stress has previously been implicating in driving TGFβ signaling [32–35], we examined cellular stress response markers in RDEB fibroblasts with or without knockdown of TSP1 and showed that reducing the level of TSP1 in RDEB fibroblasts reduced the level of the ER stress marker Glucose Regulated Protein 78 (GRP78) (*Figure 5A*). Further interrogation of the three main ER stress response pathways could not differentiate specificity in this regard; TSP1 knockdown reduced PERK, ATF6-alpha and IER1-alpha in RDEB fibroblasts (*Figure S4*). Next, and to demonstrate that ER stress and elevated levels of GRP78 correlate with increased TGFβ signaling in dermal fibroblasts, we treated normal and RDEB fibroblasts with the ER stress inducing chemicals thapsigargin and tunicamycin, demonstrating that both agents increased p-SMAD3 and GRP78 levels (*Figure 5B*). In order to

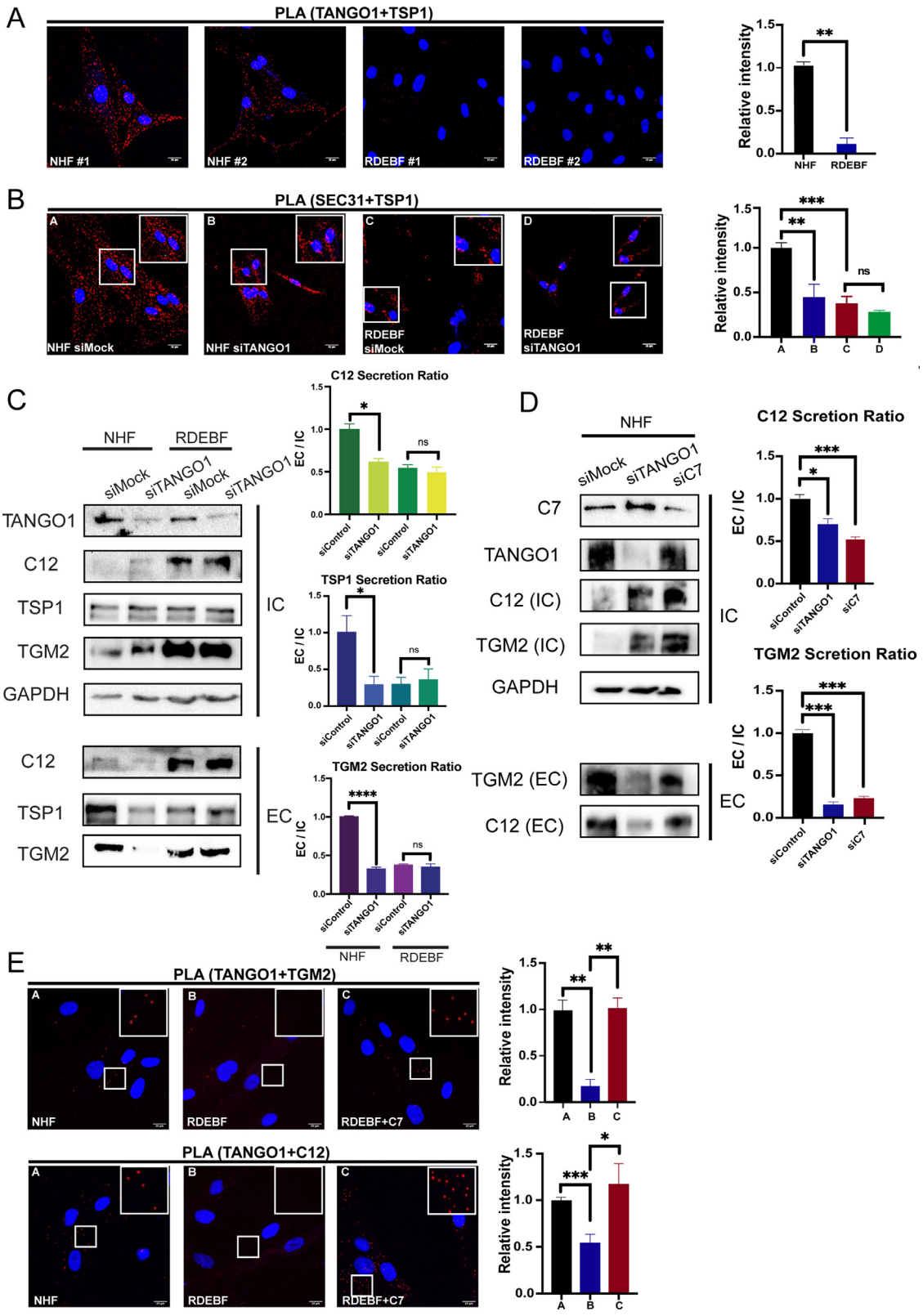

Figure 2. TANGO1 facilitates ECM-associated protein secretion in the presence of wild-type C7. (**A**) PLA showing proximity between TSP1 and TANGO1 in primary NHF and RDEBF from two separate donors. Scale bar: 20 μm. Quantification graph shows mean ± SEM signal intensity, 30 cells were counted from each replicate experiment (n=3), **: $p<0.01$. (**B**) PLA showing proximity between TSP1 and SEC31 in primary normal and RDEB fibroblast populations

confirm whether TGFβ induction by ER stress was dependent on increases of TGFβ1 ligand, we examined TGFβ1 levels and nuclear pSMAD3 in the presence of tunicamycin and the TGFBR1 inhibitor SB431542, and demonstrated that induction of TGFβ signaling in this context is independent of increases in TGFβ1 (*Figure 5C*). Finally, to confirm that intracellular levels of TSP1 correlate with TGFβ activation, we repeated these experiments using overexpression of TSP1 in the presence of SB431542 showing that indeed, intracellular TSP1 activates TGFβ signaling (*Figure 5D*). In contrast to treatment with tunicamycin, overexpression of TSP1 led to increases in TGFB1 levels and SB431542 was unable to completely blunt pSMAD3 as was the case for vector control with SB431542 (*Figure 5D*).

Discussion

Collectively, the data presented here support a model in normal dermal fibroblasts where C7 acts as a scaffold to load ECM-associated proteins via TANGO1 into large COPII carriers (*Figure 6A*, left panel). In RDEB fibroblasts, where full length, wild-type C7 is absent, proteins are trafficked through an alternate pathway associated with close proximity to C1 (*Figure 6A*, right panel). In normal dermal fibroblasts when TANGO1-C7 loading of COPII vesicles becomes saturated, protein traffics through an alternate C1-associated pathway (*Figure 6B*) leading to increased ER stress, and increased TGFβ signaling (*Figure 6C*).

Our model does not preclude trafficking through both pathways under normal, homeostatic conditions. Indeed, recent work by Rosini and colleagues identify co-localization of C1 and TSP1 in vesicle-like structures as well as proximity of C1 and TSP1 in normal dermal fibroblasts under normal culture conditions [36]. In this study (Rosini et al.), the authors demonstrate an association of TSP1 with C1, both intracellularly and extracellularly, and identify the highly conserved KGHR sequence of the collagen triple-helical domain, present in fibrillary collagens, as one of a number of collagen binding sites for TSP1 [36]. Prior work has also identified binding of TSP1 to collagen types I-V [37] but interestingly, collagen type V showed 10-fold stronger binding compared with collagens I-IV and has only one KGHR site while collagens I-III have two [37]. Our data show strong association of TSP1 to the full length, FN6/7 domain-containing C7 but does not rule out a weaker interaction with mutant, FN6/7 deleted C7 (*Figure 4*) presumably mediated through amino acid sequences separate to both FN6/7 and KGHR, as C7 does not contain a KGHR motif. Further work is needed to determine whether TSP1-C1 binding is necessary for intracellular co-localization of TSP1 and C1, and TSP1 secretion, and whether this relationship extends to other collagens.

It is also important to note the limitations of our study since much of our investigation utilizes PLA and protein-protein interactions can potentially inhibit antibody binding thereby preventing PLA even where proximity exists. However, we are confident in our data since PLA is altered consistently comparing protein manipulation, either over-expression with retrovirus, over expression via lipid transfection, or siRNA knockdown using lipid transfection, and conclusions are confirmed in primary cells from multiple separate donors, giving concordant results (n=31). It is clear to us that composition of COPII vesicles as determined by PLA differs with or without presence of C7. However, we are not tracking labelled proteins in real-time moving through normal cells and this would be the next step in validating our observations and rejecting the possibility, however slight, that retroviral expression, siRNA knockdown, and cellular response to C7 deficiency in RDEB all result in blocking formation and/or loading of TANGO1-dependent ER exit sites. Given the extent of the data presented we find this possibility highly unlikely.

Similarly, a number of studies in the literature identify TANGO1 facilitating C1 secretion and the TANGO1 knockout mouse shows perturbed collagen glycosylation, secretion, maturation, and ECM deposition yet collagens are still secreted [38]. Studies in drosophila suggest that absence of TANGO1 leads to larger proteins “clogging up” the secretory

with siRNA against TANGO1 (siTANGO1) or scrambled siRNA (siMock). Scale bar: 20 μm. Graph shows mean± SEM signal intensity from 30 cells counted from replicate experiments (n=3), **: $p < 0.01$, ***: $p<0.001$ ns: not significant. (**C**): Immunoblot of TANGO1, C12, TSP1 and TGM2 from total cell lysates (IC) and conditioned media (EC) from primary NHF and RDEBF populations treated with siMock or siTANGO1. Graph showing C12, TSP1 and TGM2 secretion levels measured by immunoblot quantification of C12 (cell media)/C12 (cell lysate), TSP1 (cell media)/TSP1 (cell lysate) and TGM2 (cell media)/TGM2 (cell lysate), with mean ± SEM from replicate experiments (n=2). **: $p<0.01$, ****: $p<0.0001$, ns: not significant. (**D**) Immunoblot of C7, TANGO1 from total cell lysate as well as C12 and TGM2 from total cell lysates (IC) and conditioned media (EC) isolated from NHF treated with siMock, C7 siRNA (siC7) or siTANGO1. Graphs show C12 and TGM2 secretion levels measured by immunoblot quantification of C12 (cell media)/C12 (cell lysate) and TGM2 (cell media)/TGM2 (cell lysate), with mean ± SEM from replicate experiments (n=3). *: $p<0.05$, ***: $p<0.001$. (**E**) PLA showing proximity between TGM2 and TANGO1, as well as C12 and TANGO1 in primary NHF, RDEBF and RDEBF overexpressing C7. Scale bar: 20 μm. Quantification graph shows mean ± SEM signal intensity of 30 cells from each replicate experiment (n=3), *: $p<0.05$, **: $p<0.01$, ***: $p<0.001$.

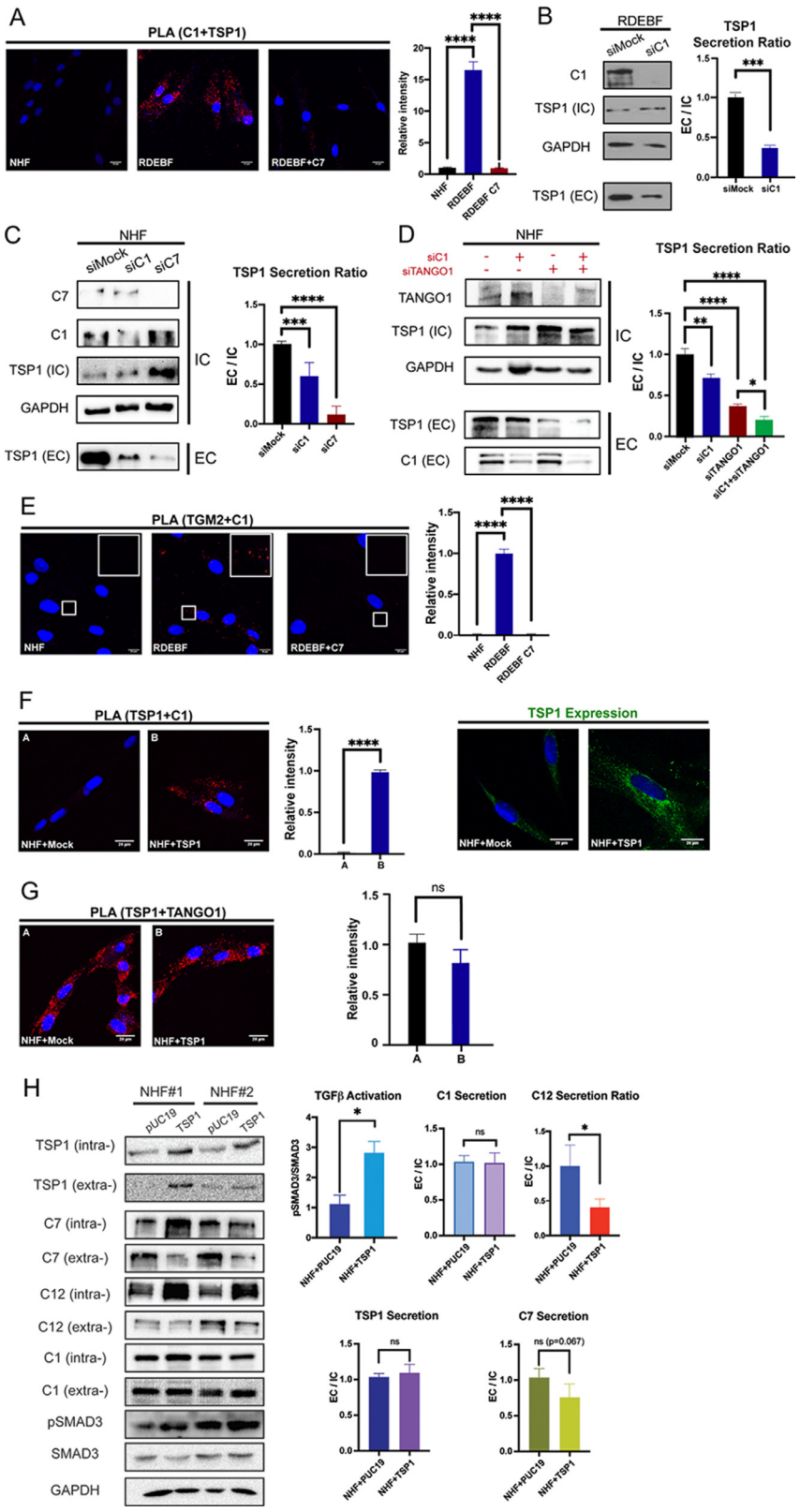

Figure 3. TSP1 secretion is associated with type I collagen when C7 is absent or when TSP1 is ectopically expressed. (**A**) Left: PLA showing proximity between TSP1 and C1 in primary NHF and RDEBF with or without recombinant C7 expression. Scale bar: 20 μm. Right: Graph shows mean ± SEM signal intensity, 30 cells were counted from

machinery and when larger proteins are also removed secretion improves [39]. More recently data report that of the two human isoforms of TANGO1, the long (TANGO1L) and short (TANGO1S) isoforms, it is TANGO1S that has a major impact on global secretion, including C1, while deleting TANGO1L has minimal effect on global secretion [20]. Since we have not deleted TANGO1 and only used siRNA depletion further work is needed to determine the role of TANGO1L and TANGO1S in the context of C7 and secretion of ECM-associated proteins.

In keeping with its involvement in a diverse range of biological functions (including cell death, signaling, cytoskeleton rearrangements, enzymatic activities, G-protein and non-enzymatic biological functions), traffic of TGM2 to both the plasma membrane and the external environment has been shown to be via multiple pathways in multiple different cellular models under various stimuli [40–42]. So-called unconventional secretion, independent of the classical ER-Golgi pathway and associated with the endosomal pathway, has been highlighted recently, and historic observations suggest that TGM2 is short lived in the ER and Golgi [43], again in cellular systems different to primary dermal fibroblasts. Here, our data show a clear role for C7 and TANGO1 in secretion of TGM2 in dermal fibroblasts and, taken together with published work, highlight tissue-specific mechanisms of secretion since C7 is not ubiquitously expressed. This is in keeping with both TSP1, since platelets do not express C7, as well as differential expression of C12, a FACIT (fibril associated collagen with intermittent repeats) collagen with a small collagenous region that interacts with fibrillar collagens through its C-terminal region [44]. TANGO1 mediated secretion of C12 was previously observed in Caco-2 cells [30], which are not known to express C7 and together our data suggest that in separate tissues, in this case human colon, other proteins are able to scaffold cargo and further work is required to fully dissect the control and sorting of cargo into COPII vesicles.

While multiple mechanisms for TGM2 traffic exist [42], our data provide a mechanism for reduced TGM2 in the dermal microenvironment of RDEB and provide a plausible explanation for disruption to autophagic flux previously identified [10]. We favor the hypothesis that disruption to TANGO1-mediated ECM-associated protein traffic in the absence of C7 provides a likely explanation to overall proteostasis perturbation in RDEB rather than a specific focus on TGM2. Indeed, accumulation of proteins within the ER-Golgi network is known to lead to cellular stress response, altered autophagy and increased TGFβ signaling [35,45].

Previous studies have reported a role for thrombospondins in mediating ER stress, including analysis of transgenic thrombospondin-4 (TSP4) expression [46] as well as cardiac specific overexpression of TSP1 [47]. The data presented here, in primary human dermal fibroblasts, suggest a role for increased TSP1 and perturbed ER-Golgi traffic in inducing all three major ER stress pathways (Figure S4). In contrast, studies of cardiac overexpression of *thbs1* leads to cardiac atrophy specifically through PERK-ATF4 regulated autophagy [47]. Studies in *thbs4* transgenic mice, and follow up work *in vitro*, describe a role for TSP4 in mediating a protective stress response, through activation of Atf6α and

each replicate experiment (n=3), ****: $p<0.0001$. (**B**) Left: Immunoblot of C1, and TSP1 from total cell lysates (IC) and conditioned media (EC) from primary RDEBF treated with scramble siRNA (siMock) or C1 siRNA (siC1). Right: Graph shows TSP1 secretion levels measured by immunoblot quantification of TSP1 (cell media)/TSP1 (cell lysate), with mean ± SEM from replicate experiments (n=3). ***: $p<0.001$. (**C**) Left: Immunoblot of C1 and C7 from total cell lysate as well as TSP1 from total cell lysates (IC) and conditioned media (EC) isolated from NHF treated with siMock, siC1 or C7 siRNA (siC7). Right: Graph shows TSP1 secretion levels measured by immunoblot quantification of TSP1 (cell media)/TSP1 (cell lysate), with mean ± SEM from replicate experiments (n=2). ***: $p<0.001$, ****: $p<0.0001$. (**D**) Left: Immunoblot of C1 from conditioned media and TANGO1 from total cell lysate as well as TSP1 from total cell lysates (IC) and conditioned media (EC) isolated from NHF treated with siMock (first column), siC1, TANGO1 siRNA (siTANGO1) or combination of both siC1 and siTANGO1. Right: Graph shows TSP1 secretion levels measured by immunoblot quantification of TSP1 (cell media)/TSP1 (cell lysate), with mean ± SEM from replicate experiments (n=3). *: $p<0.05$, **: $p<0.01$, ****: $p<0.0001$. (**E**) Left: PLA showing proximity between TGM2 and C1 in primary NHF, RDEBF and RDEBF with recombinant C7 expression. Scale bar: 20 μm. Right: Graph shows mean ± SEM signal intensity, 30 cells were counted from each replicate experiment (n=3), ****: $p<0.0001$. (**F**) Left: PLA showing proximity between TSP1 and C1 in primary NHF transiently transfected with an empty vector (NHF+Mock) or CMV-driven TSP1 vector (NHF+TSP1). Scale bar: 20 μm. Graph shows mean ± SEM PLA signal intensity, 30 cells were counted from each replicate experiment (n=3), ****: $p<0.0001$. Right: Immunostaining with anti-TSP1 antibody confirms transfection of TSP1. Scale bar: 20 μm. (**G**) Left: PLA between TSP1 and TANGO1 in NHF transiently transfected by empty vector (NHF+Mock) or CMV-driven TSP1 vector (NHF+TSP1). Scale bar: 20 μm. Right: Graph shows mean ± SEM PLA signal intensity, 30 cells were counted from each replicate experiment (n=3), ns: not significant. (**H**). Left: Immunoblot of TSP1, C7, C12 and C1 from both IC and EC, pSMAD3 and SMAD3 from IC after being transiently transfected with empty plasmid (pUC19) or TSP1 containing pUC19 vector (TSP1). GAPDH serves as loading control. Right: Graphs show mean ± SEM of TGFβ activation by quantifying the ratio of pSMAD3/SMAD3, and the secretion levels of TSP1, C7, C12 and C1 calculated by IC/EC ratios from replicate experiments (n=3). *: $p<0.05$; ns: not significant.

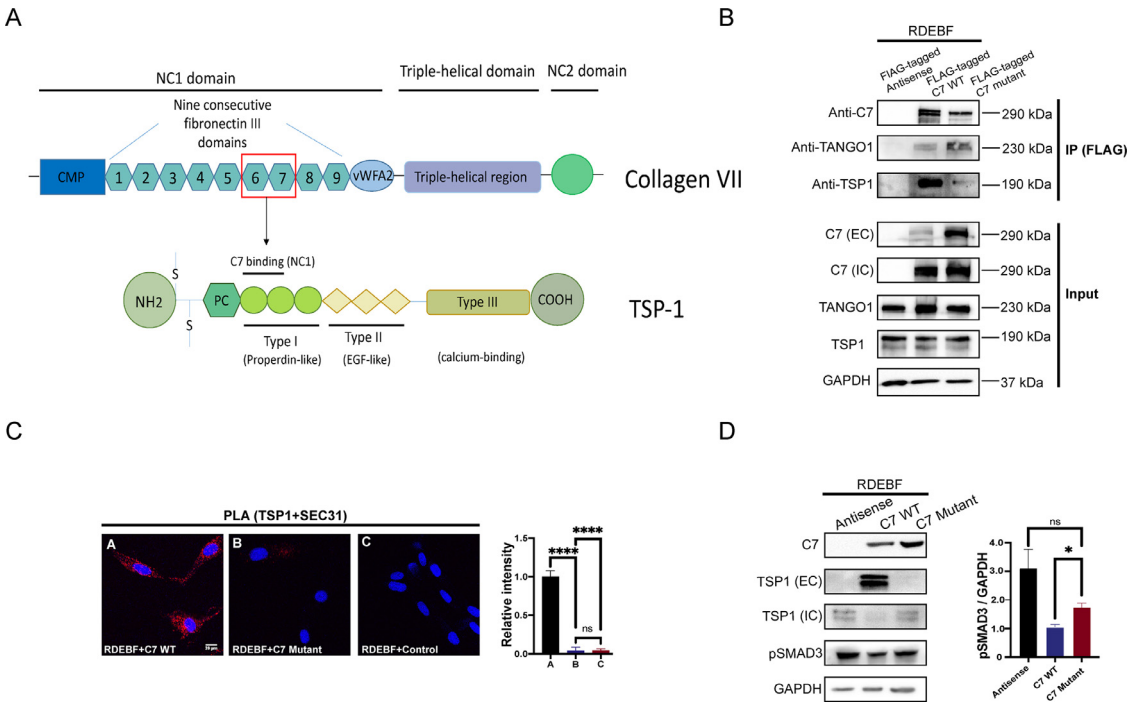

Figure 4. Binding between C7 and TSP1 promotes TSP1 secretion. (**A**) Schematic showing the structure of full-length C7 and TSP1. The reported TSP1 binding domains (FN6FN7) are indicated by the red rectangle. (**B**) Co-immunoprecipitation pulling down proteins using FLAG-tagged C7 demonstrating binding TSP1/C7 and TANGO1/C7. Proteins were detected by immunoblot with indicated antibodies. 5% of the total lysate was used for input and GAPDH was used for loading control. (**C**) Left: PLA between TSP1 and SEC31 measured in RDEBF after expression of recombinant wild-type C7, mutant C7 (ΔFN6FN7) or antisense C7 (control). Scale bars: 20 μm. Right: Graph shows mean ± SEM PLA signal intensity, 30 cells were counted from each replicate experiment (n=3), ****: $p<0.0001$, ns: not significant. (**D**) Left: Immunoblot of C7 and p-SMAD3 from total cell lysate, and TSP1 from total cell lysates (IC) and conditioned media (EC) from primary RDEBF after expression of antisense C7, recombinant wild-type C7, or mutant C7. Right: Graph shows mean ± SEM p-SMAD3 densitometry normalized to GAPDH from replicate experiments (n=3), *: $p<0.05$, ns: not significant.

GRP78 in cardiomyocytes [46,48]. Since TSP1 and TSP4 share structural homology [49], it is conceivable that increased TSP1 in dermal fibroblasts acts similarly to TSP4 in mediating a protective stress-response through interaction with ATF6α [48]. Conceptually, we favor the idea that perturbed trafficking induces ER stress with parallels to overexpression of *thbs1* in murine cardiac tissues [47] but acknowledge that further studies are required to fully dissect the relationship between TSP1 and ER stress in dermal fibroblasts.

A direct link between ER stress and TGFβ signaling has previously been reported [33,35] and evidence for a direct role of ER stress in promoting the fibrotic reaction is clear [32,34]. Here we are adding data in support of intracellular, autocrine mechanisms driving extracellular ECM disruption and future work will assess the utility of inhibitors of organelle stress, such as 4-phenylbutyric acid, for targeting both TGFβ signaling and fibrotic ECM deposition in RDEB [35,45]. The role of TSP1 in this context is intriguing since much of the prior work has focused on the ability of extracellular TSP1 bind to the latent-associated complex and release TGFβ ligand [25] while here we demonstrate a clear, intracellular role for TSP1 in TGFβ activation. Our data raise the intriguing possibility that ER-stress induced TGFβ signaling is independent from increases in TGFβ ligand and potentially canonical receptor-ligand binding but confirmation of this requires extensive work with receptor ligand deletion/ mutants and will be followed up with future studies.

In addition to TGM2 and TSP1, a handful of other proteins have been shown to be stable binding partners of C7 and of these only LH3 is reported to be secreted from the cell [10,50]. Although slight increases in extracellular LH3 were observed in RDEB fibroblasts after C7 overexpression, these were not significant and we were unable to observe PLA between SEC31 and LH3 (*Figure S5A and S5B*). These data are in agreement with LH3 associating with type IV collagen in post-Golgi vesicles in kidney epithelia cells [51].

Although RDEB is clearly a group of monogenic diseases with 100% penetrance and a defined set of

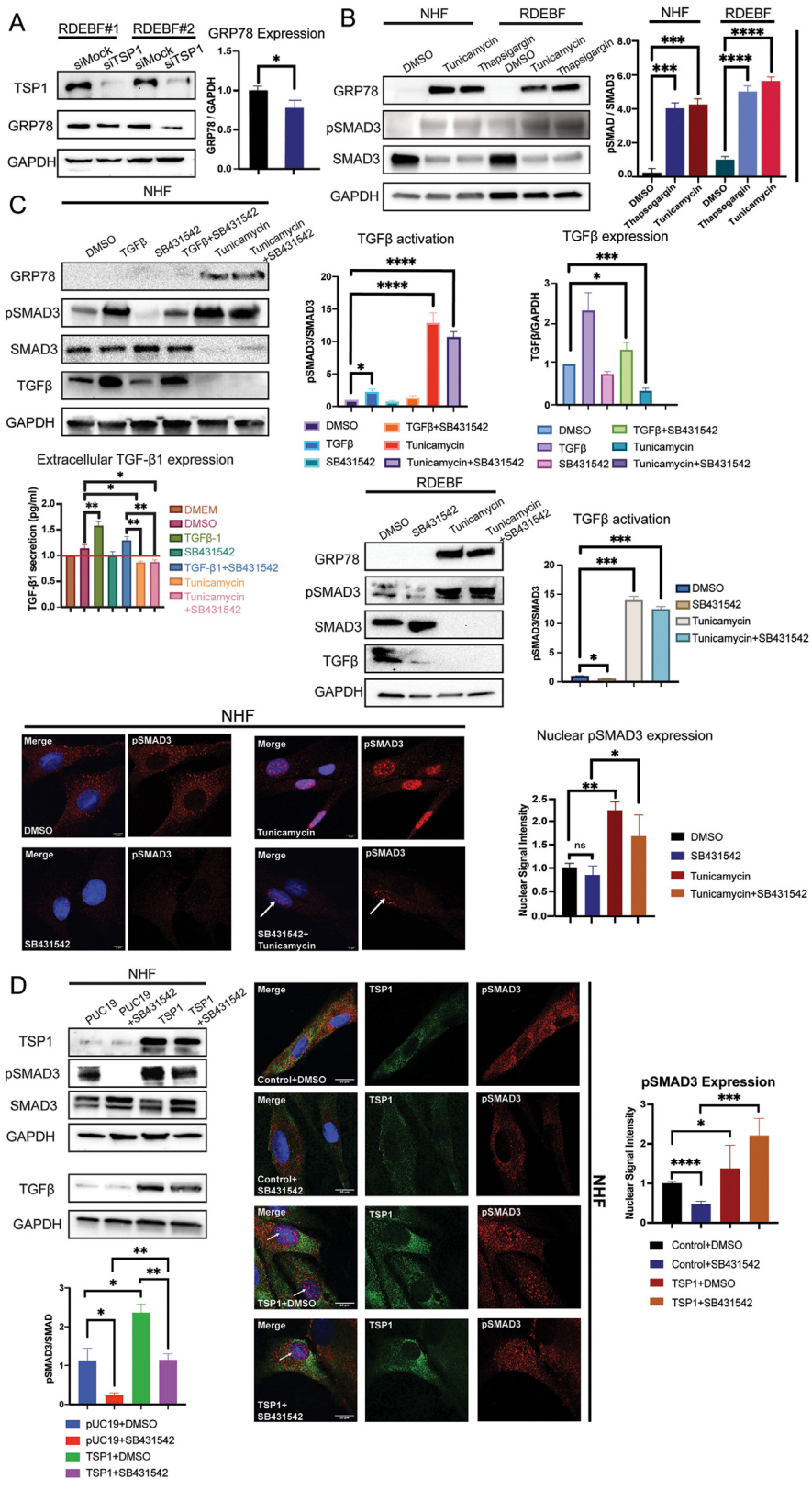

Figure 5. Intracellular TSP1 increases TGFβ signaling and ER-stress in dermal fibroblasts. (**A**) Immunoblot of TSP1 and GRP78 from total cell lysate isolated from two primary RDEBF populations treated with scrambled control (siMock) or TSP1 siRNA (siTSP1). Graph shows mean ± SEM GRP78 densitometry normalized to GAPDH from replicate

clinical criteria associated with individual disease sub-types, there is clear evidence of genetic modifiers as individual patients with the same mutations in the causative gene, *COL7A1*, can have very different disease severity and a number of potential genetic modifiers have been suggested [9,52,53]. While little consensus on the key mediators of disease severity has been reached, what is clear is that the TGFβ signaling pathway plays a role in moderating disease severity as all genetic modifiers identified to date impact TGFβ signaling in one way or another [5,9,53,54]. Furthermore, since multiple mechanisms exist for activation of TGFβ signaling and a number of these have been demonstrated to be active in RDEB cells [54] we are not proposing a single mechanism contributing to disease severity. Rather, we are adding a further mechanism for disease modification highlighting ER to Golgi traffic and ER stress as potential nodes of disease modification, which can be activated both through inability of C7 to traffic TSP1 but also indirectly through increased TSP1 expression as a result of elevated TGFβ signaling, since TSP1 is a TGFβ target.

In conclusion, we report a role for C7 in ECM-associated protein traffic and describe a mechanism for activation of cellular stress response through increased intracellular protein levels, leading to TGFβ activation. This mechanism is in addition to extracellular binding of TSP1 to LAP previously described [5] and would presumably also be prominent in chronic wounds found in patients with RDEB. Finally, our work highlights intracellular protein accumulation and consequential cellular stress response as a possible driver of carcinogenesis, since the recent overlap in gene expression profiling of RDEB SCC and head and neck SCC centers on a partial epithelial to mesenchymal transition (p-EMT) phenotype identified from single cell sequencing experiments and highlighting increased TSP1 in the tumor microenvironment [55,56].

Experimental procedures

Cell culture

The cells used in this study were isolated from skin biopsies taken as routine surgical or diagnostic procedures. Informed written consent was obtained from each patient and this study was performed in accordance with the Helsinki declaration. The cells were cultured at 37°C with 5% CO2, in Dulbecco's modified essential medium (DMEM, Corning cellgro, Mediatech, Inc Manassas, VA) which was supplemented with 10% fetal bovine serum (FBS, PEAK Serum, Cat PS-FB1, Colorado, USA) and 150μM L-ascorbic acid (catalog no. 013-12061, Wako). Normal and RDEB fibroblasts were used up to passage 7.

Antibodies

Table S1 details all antibodies used in this study.

Proximity Ligation Assay

Proximity ligation assay was performed using Duolink *in situ* Red Starter kit Mouse/Rabbit Non-haz (Duo92101, Sigma-Aldrich, St. Louis, MO) according to the manufacturer's protocol. Normal dermal human fibroblasts or RDEB fibroblasts were plated onto coverslips (Fisherbrand, Catlog No. 22293232) in 24-well plates (Corning, RED No. 3524) at 0.5×10^5 cells/well. After 48 hours, cells were fixed by 4% paraformaldehyde, permeabilized by 0.1% Triton X-100 for 10 minutes and blocked for 20 minutes at 37°C and then incubated with appropriate antibodies overnight at 4°C. After amplification of the signal, the slides were mounted and analyzed with a confocal microscope (Nikon A1R Microscope). Controls containing only a single primary antibody (omitting the paired

experiments (n=3), *: $p<0.05$. (**B**) Left: Immunoblot of GRP78, total SMAD3 and p-SMAD3 from total cell lysate isolated from primary NHF and RDEBF populations treated with DMSO (control), 0.5μM Thapsigargin or 5μg/ml Tunicamycin. Right: Graph shows mean ± SEM p-SMAD3 densitometry normalized to total SMAD3 from replicate experiments (n=3), *: $p<0.05$, **: $p<0.01$. (**C**). Upper row: Immunoblot showing total lysate levels of GRP78, pSMAD3, SMAD3 and TGFβ in NHF treated by DMSO, TGFβ recombinant protein, SB431542, TGFβ recombinant protein + SB431542, Tunicamycin, Tunicamycin + SB431542. Graphs show mean ± SEM p-SMAD3 relative to total SMAD3, TGFβ expression relative to GAPDH from replicate experiments (n=3), *: $p<0.05$, ***, $p<0.001$, ****, $p<0.0001$. Middle row: ELISA showing TGF-β1 secretion, DMEM serves as the baseline control (left graph). *: $p<0.05$, **: $p<0.01$. Immunoblot (middle) showing GRP78, pSMAD3, SMAD3 and TGFβ in RDEBF treated by DMSO. SB431542, Tunicamycin and Tunicamycin + SB431542. Graph (right) shows mean ± SEM p-SMAD3 relative to total SMAD3 from immunoblot. ***, $p<0.001$. Bottom row: Confocal images showing DAPI (blue) and pSMAD3 (red) in NHF treated with DMSO, SB431542 and SB431542+Tunicamycin. Scale bars: 10 μm. Quantification graph shows mean ± SEM nuclear signal intensity from 20 cells imaged in each replicate experiment (n=3), *: $p<0.05$, ns: not significant. (**D**). Left: Immunoblot showing TSP1, pSMAD3, SMAD3 and TGFβ expression in NHF from total lysate after transfection with empty vector (PUC19), PUC19 + SB435142, TSP1 vector and TSP1 + SB431542. Graph below shows mean ± SEM of pSMAD3 relative to SMAD3 from replicate experiments (n=3). *: $p<0.05$, **: $p<0.01$. Bottom row: Confocal images (middle) showing TSP1 (green) and pSMAD3 (red) in NHF transiently transfected with empty vector and treated with DMSO (Control+DMSO) or SB431542 (Control+ SB431542), and NHF transiently transfected with TSP1 and treated with DMSO (TSP1+DMSO) or SB431542 (TSP1+SB431542). Quantification graph (right) shows mean ± SEM nuclear signal intensity from 20 cells imaged in each replicate experiment (n=3) *: $p<0.05$, ***, $p<0.001$, ****, $p<0.0001$.

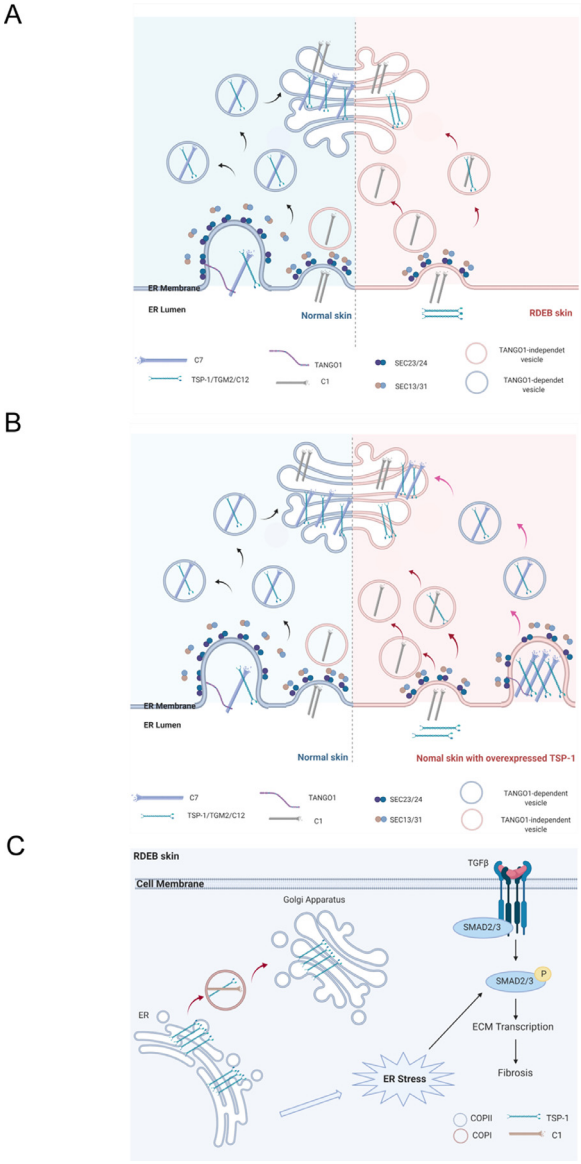

Figure 6. Model of ECM-associated protein secretion and intracellular accumulation in dermal fibroblasts. (**A**) In normal dermal fibroblasts, C7 acts as a scaffold to load the ECM-associated proteins TSP1, TGM2 and C12 via TANGO1−dependent carriers (left panel) while in RDEB dermal fibroblasts, where full length wild-type C7 is absent, ECM-associated proteins are trafficked through an alternate pathway associated with close proximity to C1 via TANGO1-independent carriers (right panel). (**B**) In normal cells when ECM-associated proteins increase to levels where the TANGO1-C7-TSP1 loading of TANGO1-dependent carriers is saturated, excess TSP1 traffics through an alternate, C1 associated pathway. (C) In situations where TSP1 is increased, intracellular TSP1 saturates both TANGO1 and C1-associated secretory pathways leading to increased ER stress and increased TGFβ signaling.

primary antibody in each case) confirmed specificity and absence of secondary PLA signals in each case.

Immunohistochemistry

Normal human fibroblasts or RDEB fibroblasts were plated on coverslips (Thomas Scientific, 6661-K40) in 6-well plates (Thermo Scientific, Catlog No. 140675) at 0.5 $\times$ 10^5 cell/well. After 48 hours, cells were fixed by 4% paraformaldehyde and blocked by 3% fetal bovine serum in 0.1% Triton X-100 for half hour at room temperature. Primary antibodies used were Collagen VII (Sigma Prestige, HPA042420, Rabbit, 1:50 dilution), Thrombospondin-1 (Santa Cruz, sc-59887, mouse, 1:50 dilution), SEC23 (Abcam, ab99552, goat, 1:100 dilution), SEC31 (Santa Cruz, sc-376587, mouse, 1:50 dilution), pSMAD3 S423/S425(Rockland, 600-401-919, Rabbit, 1:50 dilution), Calreticulin (Life Span Bioscience, LS-B5223-125, Sheep, 1:50 dilution) and Collagen I (SouthernBiotech, 1310-01, goat, 1:50). Cells with primary antibodies were incubated for 2 hours at room temperature. Secondary antibodies, Alexa Fluor 594 goat anti-rabbit (1:800) (Invitrogen, Eugene, OR), Alexa Fluor 488 goat anti-mouse (1:250) (Invitrogen, Eugene, OR), Alexa Fluor 647 donkey anti-goat (Invitrogen, Eugene, OR) and Alexa Fluor 488 donkey anti-sheep (1:250) (Invitrogen, Eugene, OR), were applied for 1 hour at room temperature. Coverslips were mounted on the slides with DAPI Fluoromount-G (SouthernBiotech, #0100-20) and analyzed by confocal microscopy (Nikon A1R Microscope).

Small Interfering RNA (siRNA) Knockdown

For siRNA knockdown of TSP1, 2 $\times$ 10^5 fibroblasts were plated in 10-cm petri-dishes (Thermo Scintific, Catlog No. 130182). The next day, the cells were transfected with SMARTpool: ON-TARGET-plus THBS1 (Catalog no. L-019743-00-0005, 5nmol), COL7A1 (L-011017-00-0005, 5nmol), COL1A1 (L-010502-00-0005, 5nmol), ON-TARGET-plus nontargeting control (L-001810-10-05, Dharmacon, Lafayette, CO) or MIA3 (TANGO1) (sc-78818, 10μM, Santa Cruz Biotechnology), using Lipofectamine 3000 (Catlog no. L3000001, Life Technologies). After 6 hours of transfection, the cells were recovered with DMEM (Corning Cellgro) supplemented with 10% fetal bovine serum (FBS) (Catlog no. PS-FB1, Peak Serum). Cells were analyzed 48 hours after transfection.

Drug treatment

SB431542 was purchased from Selleckchem (S1067, 10mM), Tunicamycin (sc-3506A, 5mg) was purchased from Santa Cruz Biotechnology and Thapsigargin (T9033-.5MG, 0.5mg) was purchased from Milipore Sigma and Human TGFβ recombinant protein (Cell signaling, #75362S, 20μg). For the ER stress measurement, cells were treated with 10μM

SB431542, 5μg/ml of tunicamycin, 0.5μM thapsigargin or DMSO and recovered with DMEM supplemented with 10% FBS after 5h treatment. Cells were harvested 24h after drug treatment. For TGFβ induction and inhibition, cells were treated with 10μM SB431542 or 5ng/ml TGFβ1 recombinant protein and harvested 48h after treatment.

Recombinant TSP1 expression

For recombinant TSP1 expression 1×10^5 fibroblasts were plated in 6-well plates (Thermo Scientific, Catlog No. 140675). The next day, the cells were transfected with THBS-1-bio-His (500ng/well) or empty pcDNA3.1 vector (500ng/well) using Lipofectamine 3000 (Catlog no. L3000001, Life Technologies). After 6 hours of transfection, the cells were recovered with DMEM (Corning Cellgro) supplemented with 10% fetal bovine serum (FBS) (Catlog no. PS-FB1, Peak Serum). Cells were analyzed 48 hours after transfection.

Recombinant wild-type C7, mutant C7 and antisense C7 by retroviral transduction

Full-length, mutated, and antisense COL7A1 (full length *COL7A1* ORF in 3'-5' orientation) were cloned into the pBabePuro vector and tagged at the C-terminus by 3xFLAG. Phoenix-Ampho cells [57] were transfected with retroviral constructs (full-length, mutated and antisense COL7A1 constructs) using Lipofectamine 3000 (Catlog no. L3000001, Life Technologies). After 48h, the virus-containing supernatant was harvested, filtered, concentrated by using Concentrator (Retro-X Concentrator, Catlog no. 631456, Takara) overnight at 4°C and used to infect target normal human or RDEB fibroblasts (1×10^5) in the presence of polybrene (8μg/ml). Two days post-infection, stable cells were selected by growth in 2μg/mL puromycin.

Protein quantification

Protein concentration in cell lysate was measured with the Pierce bicinchoninic assay Protein Assay kit (Thermo Fisher Scientific).

Co-immunoprecipitation

Primary RDEB fibroblasts stably transduced with 3xFLAG-tagged wildtype or mutant COL7A1 were lysed in RIPA buffer supplemented with protease and phosphatase inhibitors. After saving 5% of the total cell lysate for input, the extracts were subjected to immunoprecipitation with anti-FLAG Immunoprecipitation Kit (FLAGIPT1-1KT) from Millipore-Sigma, according to manufacturer's instructions. For immunoprecipitating C7, the lysates were incubated with anti-FLAG M2 affinity gel (Millipore-Sigma, A2220) overnight on a rotor, washed three times with 1X washing buffer, mixed with 25μL loading buffer containing 5% 2-mercaptoethanol and prepared for immunoblotting.

Immunoblotting

Cells were lysed in RIPA buffer supplemented with protease and phosphatase inhibitors and followed by 5-minute centrifugation at 4°C. 35-μg protein samples were loaded on 8% acrylamide gels. Primary antibodies were used at the following dilutions: TSP1 (sc-59887, Santa Cruz Biotechnology, Mouse, 1:1000 or ab85762, Abcam, rabbit, 1:2000) or (ab85762, Abcam, rabbit, 1:2000), TGM2 (sc-48387, Santa Cruz, mouse, 1:1000) or (GTX111702, GeneTex, rabbit, 1:1000), Collagen XII (sc-166020, Santa Cruz, mouse, 1:1000), C7 (234192-500UL, Milipore-sigma, Rabbit, 1:1000), C1 (1310-01, SouthernBiotech, Goat, 1:1000), TANGO1 (HPA055922, Milipore-sigma, Rabbit, 1:2000), GRP78 (sc-13539, Santa Cruz, Rat, 1:1000), p-SMAD3 (600-401-919, Rockland, Rabbit, 1:2000), polyclonal rabbit antibody raised against the NC1 domain of type VII collagen (1:8000), p-SMAD3 Ser213 (PA5-12694, Thermo Fisher, Rabbit, 1:3000), total SMAD2/3 (sc-133098, Santa Cruz, mouse, 1:2000), TGFβ (18978-1-AP, Proteintech, rabbit, 1:1000), LAMB1 (sc-374015, Santa Cruz, mouse, 1:1000), ATF6α (ab122897, Abcam, mouse, 1:2000), XBP1s (12782, cell signaling, rabbit, 1:1000), elf2α (5324, cell signaling, rabbit, 1:1000), p-elf2α Ser51 (3398, Cell Signaling, rabbit, 1:1000), SEC31 (sc-376587, Santa Cruz, Mouse, 1:1000), and GAPDH (sc-365062, Santa Cruz, Mouse, 1:3000). Resolved proteins were transferred onto nitrocellulose membrane with a BioRad Trans-Blot-Turbo, blocked in 5% milk or 5% FBS (for phosphorylated proteins) dissolved in 0.1% Tween and incubated overnight with primary antibodies. After incubation with secondary antibody (Santa Cruz Biotechnology), membrane was incubated with ECL Western blotting substrate (Thermo Fisher Scientific) and exposed to FluorChem imaging system (FluorChem E system). For protein loading, 5μg of protein was loaded for GAPDH and Collagen I. 10-25μg of protein was loaded for TSP1, pSMAD3, SEC31 and GRP78. 15-30μg of protein was loaded for Collagen VII and Collagen XII. 40μg of protein was loaded for TGM2 and TANGO1. Intracellular (IC) proteins were extracted from cell lysates and we used GAPDH as our loading control. Conditioned cell media (extracellular or EC) were collected and loaded in equivalent volumes to the cell lysates for measuring extracellular proteins. All individual Figure panels resolve IC or EC isolations from the same culture.

ELISA for detecting TGF-β1

TGF-β1 secretion was determined using a commercially available Quantikine® ELISA kit (DB100B, R&D Systems, USA). 5×10^5 normal fibroblasts or RDEB fibroblasts were cultured in 6mL of medium for 48h, in the presence and absence of TGF-β1 (5ng/ml), SB (10μM) and tunicmycin (5μg/ml) (media was removed 5h after tunicamycin treatment and cells were recovered with fresh media). 1mL of the resultant cell culture supernatant was then removed and centrifuged at 1000 g for 5 minutes. Sample supernatants were then subjected to TGF-β1 activation via a 10 minute incubation following the addition of 20 μL 1 N HCl. Samples were then neutralized with 20 μL 1.2 N NaOH/0.5 M HEPES. The ELISA was then completed according to manufactures specification, with sample TGF-β1 concentrations determined at 450 nm using a FlexStation 3 plate reader (Molecular Devices, USA), as compared to a TGF-β1 standard curve. Resultant sample concentrations are presented relative to the level of active TGF-β1 found in an FBS containing medium.

Total collagen assay

Fibroblasts were seeded at 100,000 cells/well in a six-well plate, and incubated with 3mL of 150μM L-ascorbic acid treated 10% FBS DMEM media for seven days. We used the perchlorate-free total collagen assay kit by BioVision (Catalog #: K406-100) to measure collagen in the media and cell layer (cells and extracellular matrix). We used 50μL of the media and scrapped off the cell layer in 50 μL of PBS. We used 10M NaOH to hydrolyze at 120°C for two hours to ensure complete hydrolysis followed by an equal volume of 10M HCl to neutralize. We measured the absorbance of the plate at 560 nm in the FlexStation 3 plate reader.

Nuclear protein extraction

RDEB fibroblasts were lysed according to the NE-PER® cytoplasm/nuclear protein extraction kit protocol (ThermoFisher # 78833). In brief, cells in the CER buffer reagent were centrifuged at 16,000 × *g* for 10 minutes and the cytoplasmic fraction collected. The pellet was then re-suspended in the NER buffer, centrifuged for 5 minutes at 16,000 × *g* and the nuclear protein supernatant was collected. Equal amount of proteins were loaded to 10% SDS-polyacrylamide gel for immunoblotting.

Quantitative-PCR

Total RNA was isolated using the TRIzol method (Fisher Scientific, Waltham, MA) according to the manufacturer's instructions. RNA extractions were quantified using a NanoDrop One (Fisher Scientific, Waltham, MA) and 1.5 μg RNA was used for cDNA synthesis using SuperScript III First-Strand Synthesis System (Invitrogen, Life Technologies, Carlsbad, CA). For qPCR, SYBR Select Master mix (Life technologies, Carlsbad, CA) was used and cDNA samples were diluted 1:10 to serve as a template. We used the QIAgility robot (Qiagen) for pipetting the samples and the Rotor-Gene Q for the cycler (Qiagen). Experiments were performed in duplicate due to highly accurate robot pipetting. The primers we used were from Integrated DNA Technologies (designed by OriGene) including: GAPDH Forward Sequence GTCTCCTCTGACTTCAACAGCG, Reverse Sequence ACCACCCTGTTGCTGTAGCCAA. TGF-β1 Forward Sequence TACCTGAACCCGTGTTGCTCTC, Reverse Sequence GTTGCTGAGGTATCGCCAGGAA. TGM2 Forward Sequence TGTGGCACCAAGTACCTGCTCA, Reverse Sequence GCACCTTGATGAGGTTGGACTC.

Plasmids and cloning of C7

THBS-1-bio-His was a gift from Gavin Wright (Addgene plasmid # 53417; http://n2t.net/addgene:53417; RRID: Addgene_53417). To generate 3xFLAG-tagged pBabePuro-COL7A1, we subcloned partial COL7A1 from pBabePuro-COL7A1 between the HindIII and BglII restriction sites into a pUC19-like cloning plasmid. This was followed by amplification by PCR with primers containing FLAG sequences: 5'- TGGCAGTGTTGGTCCCAGAGG – 3' and 5' - CGCCACTGTGCTGGCGAATTCGGCTTGTTAACT-CACTTGTCGTCGTCGTCCTTGTAGTC-GATGTCGTGGTCCTTGTAGTCGTCCTGGG-CAGTACCTGTCCC – 3'. The PCR product was digested with BglII and HapI and the resulting DNA fragment containing FLAG sequences was ligated back into the pUC19-like plasmid. Lastly, the PCR product in pUC19-like vector was ligated back to pBabePuro-COL7A1 between HindIII and BglII sites to generate pBabePuro-COL7A1-3xFLAG.

To delete Fn6Fn7 domains from wild-type COL7A1, we also subcloned partial 3xFLAG tagged COL7A1 into with the pBabePuro vector backbone between two AgeI sites to the pUC19-like cloning plasmid. This was followed by amplification by PCR to delete the Fn6Fn7 domains with 5'- ACGCCAGGGTTTTCCCAGTC –3' as the forward primer and 5'- CGCCTCAGCGAGTGCTCCCCGCGCTGCACCACGTGAAGCGTCCCCAGGGCTGGCGGAGCCTCAGGCGGCGTAGTGACAACAATGGAGACGTCCGTTCGAGCCACGATGAC – 3' as the

reverse primer. The PCR product was digested with NdeI and BbvCI and the resulting DNA fragment without the Fn6Fn7 domains was ligated back into the pUC19-like plasmid. Lastly, the subcloned pUC19-like plasmid was digested and ligated back to pBabePuro-COL7A1-3xFLAG between two AgeI restriction sites to generate pBabePuro-COL7A1 ΔFn6Fn7-3xFLAG.

Statistics

Unless specified, all experiments were independently performed three times. Significance was determined by GraphPad Prism using a two-tailed Student's t-test if the normality assumption was met or Mann-Whitney U-test if otherwise. $P \leq 0.05$ was considered significant and represented with a *, $p \leq 0.01$ was represented with **, $p \leq 0.001$ was represented with *** and $p \leq 0.0001$ was represented with ****.

Data Availability

All study data are included in the article and/or supporting information.

Author Contributions

Conceptualization, A.P.S; Methodology, A.P.S and Q.C; Investigation, Q.C, G.T, S.P, M.A., P.H.P, and M.F; Writing – Original Draft, A.P.S and Q.C.; Writing – Review & Editing, all authors; Funding Acquisition, A.P.S; Resources, A.P.S, I.F, M.C, J.A. M, F.P and J.S-A; Supervision, A.P.S

Competing Interest Statement

A.P.S. holds stock in Krystal Biotech Inc. and consults for and has ownership interests in Zikani Therapeutics.

Acknowledgments

This work was supported by the Office of the Assistant Secretary of Defense for Health Affairs and the Defense Health Agency J9, Research and Development Directorate, through the Congressionally Directed Medical Research Program under Award No. W81XWH-18-1-0382; and in part by the EB Research Partnership, The EB Medical Research Foundation, and the National Cancer Institute of the National Institutes of Health, Award No. R01 CA244522. Opinions, interpretations, conclusions and recommendations are those of the authors and are not necessarily endorsed by the Department of Defense or the NIH. We would like to thank all the patients who contributed to this study and the Microscopy Shared Resource at the Sidney Kimmel Cancer Center, supported by the NCI, grant 5P30CA056036-17. Figures 6 and S1 are created with BioRender.com.

Supplementary materials

Supplementary material associated with this article can be found, in the online version, at doi:10.1016/j.matbio.2022.06.008.

Received 15 February 2022;
Received in revised form 15 June 2022;
Accepted 27 June 2022
Available online 30 June 2022

Keywords:
Collagen VII;
thrombospondin;
recessive dystrophic epidermolysis bullosa;
TANGO1;
ER stress;
and TGFβ signaling

Abbreviations:
C7, collagen VII; TSP1, Thrombospondin1; C1, collagen I, RDEB, recessive dystrophic epidermolysis bullosa; TANGO1, Transport ANd Golgi Organization-1; COPII, COat Protein complex II

References

[1] A.M. Christiano, G. Anhalt, S. Gibbons, E.A. Bauer, J. Uitto, Premature termination codons in the type VII collagen gene (COL7A1) underlie severe, mutilating recessive dystrophic epidermolysis bullosa, Genomics 21 (1) (1994) 160–168.
[2] J.D. Fine, L. Bruckner-Tuderman, R.A. Eady, E.A. Bauer, J.W. Bauer, C. Has, A. Heagerty, H. Hintner, A. Hovnanian, M.F. Jonkman, I. Leigh, M.P. Marinkovich, A.E. Martinez, J.A. McGrath, J.E. Mellerio, C. Moss, D.F. Murrell, H. Shimizu, J. Uitto, D. Woodley, G. Zambruno, Inherited epidermolysis bullosa: updated recommendations on diagnosis and classification, J Am Acad Dermatol 70 (6) (2014) 1103–1126.
[3] J.D. Fine, L.B. Johnson, M. Weiner, K.P. Li, C. Suchindran, Epidermolysis bullosa and the risk of life-threatening cancers: the National EB Registry experience, 1986-2006, J Am Acad Dermatol 60 (2) (2009) 203–211.
[4] R.E. Burgeson, Type VII collagen, anchoring fibrils, and epidermolysis bullosa, J Invest Dermatol 101 (3) (1993) 252–255.
[5] V.S. Atanasova, R.J. Russell, T.G. Webster, Q. Cao, P. Agarwal, Y.Z. Lim, S. Krishnan, I. Fuentes, C. Guttmann-Gruber, J.A. McGrath, J.C. Salas-Alanis, A. Fertala, A.P. South, Thrombospondin-1 Is a Major

Activator of TGF-beta Signaling in Recessive Dystrophic Epidermolysis Bullosa Fibroblasts, J Invest Dermatol 139 (7) (2019) 1497-1505 e5.
[6] V. Kuttner, C. Mack, K.T. Rigbolt, J.S. Kern, O. Schilling, H. Busch, L. Bruckner-Tuderman, J. Dengjel, Global remodelling of cellular microenvironment due to loss of collagen VII, Mol Syst Biol 9 (2013) 657.
[7] Y.Z. Ng, C. Pourreyron, J.C. Salas-Alanis, J.H. Dayal, R. Cepeda-Valdes, W. Yan, S. Wright, M. Chen, J.D. Fine, F.J. Hogg, J.A. McGrath, D.F. Murrell, I.M. Leigh, E.B. Lane, A.P. South, Fibroblast-derived dermal matrix drives development of aggressive cutaneous squamous cell carcinoma in patients with recessive dystrophic epidermolysis bullosa, Cancer Res 72 (14) (2012) 3522–3534.
[8] A. Nystrom, D. Velati, V.R. Mittapalli, A. Fritsch, J.S. Kern, L. Bruckner-Tuderman, Collagen VII plays a dual role in wound healing, J Clin Invest 123 (8) (2013) 3498–3509.
[9] T. Odorisio, M. Di Salvio, A. Orecchia, G. Di Zenzo, E. Piccinni, F. Cianfarani, A. Travaglione, P. Uva, B. Bellei, A. Conti, G. Zambruno, D. Castiglia, Monozygotic twins discordant for recessive dystrophic epidermolysis bullosa phenotype highlight the role of TGF-beta signalling in modifying disease severity, Hum Mol Genet 23 (15) (2014) 3907–3922.
[10] V. Kuttner, C. Mack, C. Gretzmeier, L. Bruckner-Tuderman, J. Dengjel, Loss of collagen VII is associated with reduced transglutaminase 2 abundance and activity, J Invest Dermatol 134 (9) (2014) 2381–2389.
[11] K. Thriene, B.A. Gruning, O. Bornert, A. Erxleben, J. Leppert, I. Athanasiou, E. Weber, D. Kiritsi, A. Nystrom, T. Reinheckel, R. Backofen, C. Has, L. Bruckner-Tuderman, J. Dengjel, Combinatorial Omics Analysis Reveals Perturbed Lysosomal Homeostasis in Collagen VII-deficient Keratinocytes, Mol Cell Proteomics 17 (4) (2018) 565–579.
[12] A. Nystrom, O. Bornert, T. Kuhl, C. Gretzmeier, K. Thriene, J. Dengjel, A. Pfister-Wartha, D. Kiritsi, L. Bruckner-Tuderman, Impaired lymphoid extracellular matrix impedes antibacterial immunity in epidermolysis bullosa, Proc Natl Acad Sci U S A 115 (4) (2018) E705–E714.
[13] M.D. Shoulders, R.T. Raines, Collagen structure and stability, Annu Rev Biochem 78 (2009) 929–958.
[14] K. Saito, M. Chen, F. Bard, S. Chen, H. Zhou, D. Woodley, R. Polischuk, R. Schekman, V. Malhotra, TANGO1 facilitates cargo loading at endoplasmic reticulum exit sites, Cell 136 (5) (2009) 891–902.
[15] K. Saito, T. Katada, Mechanisms for exporting large-sized cargoes from the endoplasmic reticulum, Cell Mol Life Sci 72 (19) (2015) 3709–3720.
[16] L. Jin, K.B. Pahuja, K.E. Wickliffe, A. Gorur, C. Baumgartel, R. Schekman, M. Rape, Ubiquitin-dependent regulation of COPII coat size and function, Nature 482 (7386) (2012) 495–500.
[17] C. Nogueira, P. Erlmann, J. Villeneuve, A.J. Santos, E. Martinez-Alonso, J.A. Martinez-Menarguez, V. Malhotra, SLY1 and Syntaxin 18 specify a distinct pathway for procollagen VII export from the endoplasmic reticulum, Elife 3 (2014) e02784.
[18] J. McCaughey, N.L. Stevenson, S. Cross, D.J. Stephens, ER-to-Golgi trafficking of procollagen in the absence of large carriers, J Cell Biol 218 (3) (2019) 929–948.
[19] J. Peotter, W. Kasberg, I. Pustova, A. Audhya, COPII-mediated trafficking at the ER/ERGIC interface, Traffic 20 (7) (2019) 491–503.
[20] J. McCaughey, N.L. Stevenson, J.M. Mantell, C.R. Neal, A. Paterson, K. Heesom, D.J. Stephens, A general role for TANGO1, encoded by MIA3, in secretory pathway organization and function, J Cell Sci 134 (17) (2021).
[21] L. Yuan, S.J. Kenny, J. Hemmati, K. Xu, R. Schekman, TANGO1 and SEC12 are copackaged with procollagen I to facilitate the generation of large COPII carriers, Proc Natl Acad Sci U S A 115 (52) (2018) E12255–E12264.
[22] M. D'Eletto, M.G. Farrace, L. Falasca, V. Reali, S. Oliverio, G. Melino, M. Griffin, G.M. Fimia, M. Piacentini, Transglutaminase 2 is involved in autophagosome maturation, Autophagy 5 (8) (2009) 1145–1154.
[23] F. Rossin, M. D'Eletto, D. Macdonald, M.G. Farrace, M. Piacentini, TG2 transamidating activity acts as a reostat controlling the interplay between apoptosis and autophagy, Amino Acids 42 (5) (2012) 1793–1802.
[24] A. Resovi, D. Pinessi, G. Chiorino, G. Taraboletti, Current understanding of the thrombospondin-1 interactome, Matrix Biol 37 (2014) 83–91.
[25] J.E. Murphy-Ullrich, Thrombospondin 1 and Its Diverse Roles as a Regulator of Extracellular Matrix in Fibrotic Disease, J Histochem Cytochem 67 (9) (2019) 683–699.
[26] S.E. Crawford, V. Stellmach, J.E. Murphy-Ullrich, S.M. Ribeiro, J. Lawler, R.O. Hynes, G.P. Boivin, N. Bouck, Thrombospondin-1 is a major activator of TGF-beta1 in vivo, Cell 93 (7) (1998) 1159–1170.
[27] J.E. Nor, L. Dipietro, J.E. Murphy-Ullrich, R.O. Hynes, J. Lawler, P.J. Polverini, Activation of Latent TGF-beta1 by Thrombospondin-1 is a Major Component of Wound Repair, Oral Biosci Med 2 (2) (2005) 153–161.
[28] S. Schultz-Cherry, H. Chen, D.F. Mosher, T.M. Misenheimer, H.C. Krutzsch, D.D. Roberts, J.E. Murphy-Ullrich, Regulation of transforming growth factor-beta activation by discrete sequences of thrombospondin 1, J Biol Chem 270 (13) (1995) 7304–7310.
[29] I. Weibrecht, K.J. Leuchowius, C.M. Clausson, T. Conze, M. Jarvius, W.M. Howell, M. Kamali-Moghaddam, O. Soderberg, Proximity ligation assays: a recent addition to the proteomics toolbox, Expert Rev Proteomics 7 (3) (2010) 401–409.
[30] A.J. Santos, C. Nogueira, M. Ortega-Bellido, V. Malhotra, TANGO1 and Mia2/cTAGE5 (TALI) cooperate to export bulky pre-chylomicrons/VLDLs from the endoplasmic reticulum, J Cell Biol 213 (3) (2016) 343–354.
[31] S. Aho, J. Uitto, Two-hybrid analysis reveals multiple direct interactions for thrombospondin 1, Matrix Biol 17 (6) (1998) 401–412.
[32] H. Tanjore, W.E. Lawson, T.S. Blackwell, Endoplasmic reticulum stress as a pro-fibrotic stimulus, Biochim Biophys Acta 1832 (7) (2013) 940–947.
[33] M. Kassan, M. Galan, M. Partyka, Z. Saifudeen, D. Henrion, M. Trebak, K. Matrougui, Endoplasmic reticulum stress is involved in cardiac damage and vascular endothelial dysfunction in hypertensive mice, Arterioscler Thromb Vasc Biol 32 (7) (2012) 1652–1661.
[34] W.E. Lawson, D.S. Cheng, A.L. Degryse, H. Tanjore, V.V. Polosukhin, X.C. Xu, D.C. Newcomb, B.R. Jones, J. Roldan, K.B. Lane, E.E. Morrisey, M.F. Beers, F.E. Yull, T.S. Blackwell, Endoplasmic reticulum stress enhances fibrotic remodeling in the lungs, Proc Natl Acad Sci U S A 108 (26) (2011) 10562–10567.
[35] K.A. Zimmerman, L.V. Graham, M.A. Pallero, J.E. Murphy-Ullrich, Calreticulin regulates transforming growth factor-beta-stimulated extracellular matrix production, J Biol Chem 288 (20) (2013) 14584–14598.

[36] S. Rosini, N. Pugh, A.M. Bonna, D.J.S. Hulmes, R.W. Farndale, J.C. Adams, Thrombospondin-1 promotes matrix homeostasis by interacting with collagen and lysyl oxidase precursors and collagen cross-linking sites, Sci Signal 11 (532) (2018).
[37] N.J. Galvin, P.M. Vance, V.M. Dixit, B. Fink, W.A. Frazier, Interaction of human thrombospondin with types I-V collagen: direct binding and electron microscopy, J Cell Biol 104 (5) (1987) 1413–1422.
[38] D.G. Wilson, K. Phamluong, L. Li, M. Sun, T.C. Cao, P.S. Liu, Z. Modrusan, W.N. Sandoval, L. Rangell, R.A. Carano, A.S. Peterson, M.J. Solloway, Global defects in collagen secretion in a Mia3/TANGO1 knockout mouse, J Cell Biol 193 (5) (2011) 935–951.
[39] L.D. Rios-Barrera, S. Sigurbjornsdottir, M. Baer, M. Leptin, Dual function for Tango1 in secretion of bulky cargo and in ER-Golgi morphology, Proc Natl Acad Sci U S A 114 (48) (2017) E10389–E10398.
[40] G. Furini, N. Schroeder, L. Huang, D. Boocock, A. Scarpellini, C. Coveney, E. Tonoli, R. Ramaswamy, G. Ball, C. Verderio, T.S. Johnson, E.A.M. Verderio, Proteomic Profiling Reveals the Transglutaminase-2 Externalization Pathway in Kidneys after Unilateral Ureteric Obstruction, J Am Soc Nephrol 29 (3) (2018) 880–905.
[41] M. Piacentini, M. D'Eletto, M.G. Farrace, C. Rodolfo, F. Del Nonno, G. Ippolito, L. Falasca, Characterization of distinct sub-cellular location of transglutaminase type II: changes in intracellular distribution in physiological and pathological states, Cell Tissue Res 358 (3) (2014) 793–805.
[42] E.A. Zemskov, I. Mikhailenko, R.C. Hsia, L. Zaritskaya, A.M. Belkin, Unconventional secretion of tissue transglutaminase involves phospholipid-dependent delivery into recycling endosomes, PLoS One 6 (4) (2011) e19414.
[43] L. Lorand, R.M. Graham, Transglutaminases: crosslinking enzymes with pleiotropic functions, Nat Rev Mol Cell Biol 4 (2) (2003) 140–156.
[44] D.R. Keene, G.P. Lunstrum, N.P. Morris, D.W. Stoddard, R.E. Burgeson, Two type XII-like collagens localize to the surface of banded collagen fibrils, J Cell Biol 113 (4) (1991) 971–978.
[45] S.F. de Almeida, G. Picarote, J.V. Fleming, M. Carmo-Fonseca, J.E. Azevedo, M. de Sousa, Chemical chaperones reduce endoplasmic reticulum stress and prevent mutant HFE aggregate formation, J Biol Chem 282 (38) (2007) 27905–27912.
[46] J.M. Lynch, M. Maillet, D. Vanhoutte, A. Schloemer, M.A. Sargent, N.S. Blair, K.A. Lynch, T. Okada, B.J. Aronow, H. Osinska, R. Prywes, J.N. Lorenz, K. Mori, J. Lawler, J. Robbins, J.D. Molkentin, A thrombospondin-dependent pathway for a protective ER stress response, Cell 149 (6) (2012) 1257–1268.
[47] D. Vanhoutte, T.G. Schips, A. Vo, K.M. Grimes, T.A. Baldwin, M.J. Brody, F. Accornero, M.A. Sargent, J.D. Molkentin, Thbs1 induces lethal cardiac atrophy through PERK-ATF4 regulated autophagy, Nat Commun 12 (1) (2021) 3928.
[48] M.J. Brody, T.G. Schips, D. Vanhoutte, O. Kanisicak, J. Karch, B.D. Maliken, N.S. Blair, M.A. Sargent, V. Prasad, J.D. Molkentin, Dissection of Thrombospondin-4 Domains Involved in Intracellular Adaptive Endoplasmic Reticulum Stress-Responsive Signaling, Mol Cell Biol 36 (1) (2016) 2–12.
[49] J.C. Adams, Matricellular Proteins: Functional Insights From Non-mammalian Animal Models, Curr Top Dev Biol 130 (2018) 39–105.
[50] S.A. Watt, J.H. Dayal, S. Wright, M. Riddle, C. Pourreyron, J.R. McMillan, R.M. Kimble, M. Prisco, U. Gartner, E. Warbrick, W.H. McLean, I.M. Leigh, J.A. McGrath, J.C. Salas-Alanis, J. Tolar, A.P. South, Lysyl Hydroxylase 3 Localizes to Epidermal Basement Membrane and Is Reduced in Patients with Recessive Dystrophic Epidermolysis Bullosa, PLoS One 10 (9) (2015) e0137639.
[51] B. Banushi, F. Forneris, A. Straatman-Iwanowska, A. Strange, A.M. Lyne, C. Rogerson, J.J. Burden, W.E. Heywood, J. Hanley, I. Doykov, K.R. Straatman, H. Smith, D. Bem, J. Kriston-Vizi, G. Ariceta, M. Risteli, C. Wang, R.E. Ardill, M. Zaniew, J. Latka-Grot, S.N. Waddington, S.J. Howe, F. Ferraro, A. Gjinovci, S. Lawrence, M. Marsh, M. Girolami, L. Bozec, K. Mills, P. Gissen, Regulation of post-Golgi LH3 trafficking is essential for collagen homeostasis, Nat Commun 7 (2016) 12111.
[52] C. Bodemer, S.I. Tchen, S. Ghomrasseni, S. Seguier, F. Gaultier, S. Fraitag, Y. de Prost, G. Godeau, Skin expression of metalloproteinases and tissue inhibitor of metalloproteinases in sibling patients with recessive dystrophic epidermolysis and intrafamilial phenotypic variation, J Invest Dermatol 121 (2) (2003) 273–279.
[53] M. Titeux, V. Pendaries, L. Tonasso, A. Decha, C. Bodemer, A. Hovnanian, A frequent functional SNP in the MMP1 promoter is associated with higher disease severity in recessive dystrophic epidermolysis bullosa, Hum Mutat 29 (2) (2008) 267–276.
[54] E. Akasaka, S. Kleiser, G. Sengle, L. Bruckner-Tuderman, A. Nystrom, Diversity of Mechanisms Underlying Latent TGF-beta Activation in Recessive Dystrophic Epidermolysis Bullosa, J Invest Dermatol (2020).
[55] R.J. Cho, L.B. Alexandrov, N.Y. den Breems, V.S. Atanasova, M. Farshchian, E. Purdom, T.N. Nguyen, C. Coarfa, K. Rajapakshe, M. Prisco, J. Sahu, P. Tassone, E.J. Greenawalt, E.A. Collisson, W. Wu, H. Yao, X. Su, C. Guttmann-Gruber, J.P. Hofbauer, R. Hashmi, I. Fuentes, S.C. Benz, J. Golovato, E.A. Ehli, C.M. Davis, G.E. Davies, K.R. Covington, D.F. Murrell, J.C. Salas-Alanis, F. Palisson, A.L. Bruckner, W. Robinson, C. Has, L. Bruckner-Tuderman, M. Titeux, M.F. Jonkman, E. Rashidghamat, S.M. Lwin, J.E. Mellerio, J.A. McGrath, J.W. Bauer, A. Hovnanian, K.Y. Tsai, A.P. South, APOBEC mutation drives early-onset squamous cell carcinomas in recessive dystrophic epidermolysis bullosa, Sci Transl Med 10 (455) (2018).
[56] S.V. Puram, I. Tirosh, A.S. Parikh, A.P. Patel, K. Yizhak, S. Gillespie, C. Rodman, C.L. Luo, E.A. Mroz, K.S. Emerick, D.G. Deschler, M.A. Varvares, R. Mylvaganam, O. Rozenblatt-Rosen, J.W. Rocco, W.C. Faquin, D.T. Lin, A. Regev, B.E. Bernstein, Single-Cell Transcriptomic Analysis of Primary and Metastatic Tumor Ecosystems in Head and Neck Cancer, Cell 171 (7) (2017) 1611-1624 e24.
[57] T.M. Kinsella, G.P. Nolan, Episomal vectors rapidly and stably produce high-titer recombinant retrovirus, Hum Gene Ther 7 (12) (1996) 1405–1413.